Available online at www.sciencedirect.com

ScienceDirect

International Journal of Solids and Structures 43 (2006) 7659–7672

INTERNATIONAL JOURNAL OF SOLIDS and STRUCTURES

www.elsevier.com/locate/ijsolstr

Mullins effect in elastomers filled with particles aligned by a magnetic field

E. Coquelle, G. Bossis *

LPMC, UMR6622, University of Nice Sophia-Antipolis, Parc Valrose, 06108 Nice-Cedex 2, France

Received 22 November 2005; received in revised form 10 March 2006
Available online 28 March 2006

Abstract

Magnetorheological elastomers (MRE) are particulate composite materials, whose fillers are structured by a magnetic field during curing. These particles are brought in quasi-contact by the field, in a chain-like unidirectional structure. Due to this organization the local stresses between the particles is high and debonding between particles and elastomer occur at low strain. We have experimentally studied and analytically modeled the progressive breaking of the polymer-to-particle bonds. The two cases of strong and weak bonds between elastomers and particles have been studied. The analytical model correctly reproduces the stress strain curve in the presence of a debonding process although overestimating the size of the debonding cavity which is obtained by comparison between experiments and FEM simulations. The extension of the model to a chain of spheres allows to well explain the Mullins effect on MRE. Furthermore it is shown that the quality of the bonds between the particles and the elastomer does not influence the change of stiffness brought by the application of a magnetic field.

Keywords: Filled elastomers; Debonding; Mullins effect; Magnetorheological elastomers

1. Introduction

Filled rubbers are used in a large range of industrial applications, mostly dealing with damping. However, their mechanical properties are set once and for all during their elaboration process. A new way consists in using magnetic particles to create a so-called magnetorheological elastomer (MRE). It allows new applications, like engine mounts, shock absorbers, seat damping, etc., thanks to its ability to rapidly and reversibly change its rheological properties once a magnetic field is applied (Sohoni and Mark, 1987; Carlson and Jolly, 2000; Ginder et al., 1999; Bellan and Bossis, 2002; Occhiuzzi et al., 2003).

Most of the papers related to magnetorheological elastomers deal with the effect of the magnetic field on elastic properties or on other adaptive properties like magnetostriction, according to Bossis et al. (2004). In this paper we wish to use the advantage related to a quite simple organisation of the filler particles to study

* Corresponding author. Tel.: +33 492076775; fax: +33 492076754.
E-mail address: Bossis@unice.fr (G. Bossis).

0020-7683/$ - see front matter
doi:10.1016/j.ijsolstr.2006.03.020

the effect of debonding during the first traction on the final elasticity modulus of the material. So this paper will focus on the Mullins effect which is highly enhanced in comparison with the one of usual isotropic materials. The key point is that in MRE, the particles are in quasi-contact inside a chain. Thus, during stretching, one quickly reaches high local stresses (in the gap area between two adjacent particles) and favours the detachment of the polymer from the particles through a debonding process. Recently, Coquelle et al., in press have shown that it was possible to deduce the average gap between particles from traction measurements of the stress/strain curve.

In Section 2, we shall propose an analytical model for debonding, which will be compared to the experimental stress/strain curves obtained onto a two spheres system. In Section 3, this model will be extended to the case of a structured composite and its prediction compared with experimental uniaxial traction curves realized on such samples.

2. Two spheres cell

The description of the structured composite involves at least two parameters, even if we assume that this material is made of perfect, defect-less chains: the gap between two neighbour particles inside a chain, and the adhesion energy between the polymer and the particles. Following the same procedure described in Coquelle et al., in press, we shall use experiments made on two macroscopic spheres of radius $a = 1$ cm, where the gap is known in order to compare with analytical model or FEM simulations.

During uniaxial tensions, we expect that the maximum local stress in the elastomer is located at the vicinity of the poles of the spheres, leading to a detachment of the polymer matrix from the particles (provided the polymer-to-particle bonds are weaker than the polymer-to-polymer bonds). This process, called debonding, has been extensively studied in the 1980s by Gent (1980), Gent and Park (1984), and more recently by Zhuk et al. (1993), Kraus et al. (1997), Huang and Korobeinik (2001). Meanwhile, Moshev and his co-workers published in 1997, 2000 and 2002 the evolution of the local stresses inside an elementary cell using FEM simulations.

In this section, we first present an analytical model for debonding between two spheres. In this situation, elastomer is present only between them, thus letting the border located in $r = a$ free to move (Fig. 1). In order to check the analytical model's hypothesis, finite element simulations have been used. They are based on axisymmetric, hyperelastic element, with four degrees of liberty (X, Y, Z and the hydrostatic pressure), taking into account the non-linear behaviour of the elastomer (fitted with a five parameters Mooney–Rivlin law including its Young modulus and Poisson ratio $\upsilon = 0.493$). The examination of the local stress, especially for a weakly bonded elastomer, will give useful information on the cavity initiation and growth, whereas the overall stress will be used for a comparison with the analytical model. We shall compare the predictions of this analytical model to experimental results obtained on two macroscopic iron spheres, either uncoated or coated (strong polymer to particle bonds). In the following, we shall often use the local strain: $\varepsilon_{\text{gap}} = u/g = \varepsilon(1 + 2a/g)$ which plays the major rôle for debonding criteria.

2.1. Model of debonding between two spheres

The modelling involves three steps: a stress/strain relationship before the initiation of any damage, a criteria predicting the creation and the growth of a debonded area, a stress/strain relationship for the two spheres system with a debonded area inside.

2.1.1. Mechanical behaviour before debonding

It has been shown that, in the frame of linear elasticity, this two spheres system could be described by an effective modulus approach, following Christensen (1979). He solved the mechanical equilibrium using the lubrication approximation, requiring the gap between the spheres being much smaller than the inclusion radius. In the absence of debonding the effective modulus of the two-spheres cell is:

$$E_{\text{eff}} = \frac{1}{4} E_{\text{m}} \frac{(2a+g)}{a} \int_0^{\frac{\pi}{2}} \frac{\sin^3\theta\cos\theta}{(g/2a + 1 - \cos\theta)^3} \mathrm{d}\theta \tag{1}$$

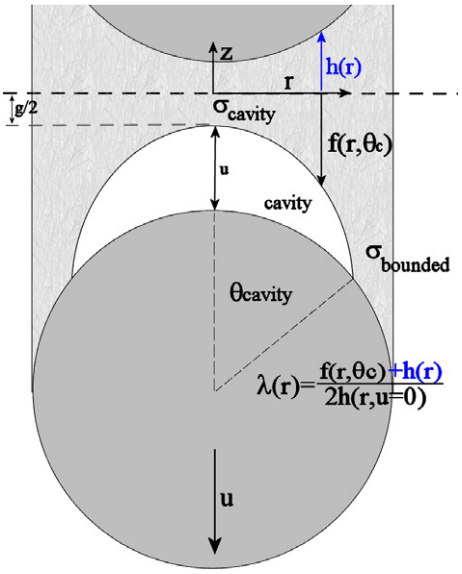

Fig. 1. The two spheres cell. At zero strain the gap is g. For a displacement, u, the shape of the cavity is defined by the function $f(r, \theta_c)$, cf. Eq. (7).

which can be approximated, for $g \to 0$ by:

$$E_{\text{eff}} = \frac{3}{4} E_{\text{m}} \frac{2a+g}{g} \tag{2}$$

where E_{m} is the Young modulus of the elastomer matrix. Of course as the gap decreases, the effective modulus will not tend to infinity since the elastomer will either debond or break, that is what we are going to see in the following section.

2.1.2. Debonding criteria

As the strain is increased, the detachment of the elastomeric matrix from the spheres takes place as soon as the local elastic energy released by the matrix overcomes the energy needed to create a new surface, and hence to propagate debonding. This is a direct application of the Griffith failure criterion, as described in Kendall (1994). In the following discussion, the linear elasticity will still be used, and the debonded area will be characterized by an angle θ_{cavity} (Fig. 1). Assuming a zero-strain energy density in the immediate vicinity of the debonded area and an unchanged one elsewhere, Gent (1980) has proposed a criterion that gives the local stress needed to propagate the cavity up to the angle θ_{cavity}. He assumes that the volume of the debonded zone is:

$$\Delta V = k(a \sin \theta_{\text{cavity}})^3 \tag{3}$$

where k is an adimensional quantity equal to 2. It has been calculated a posteriori by comparing the criteria value σ_c to a full calculation of a circular detachment at the vicinity of a plate, for small θ. The value of k has been given by Mossakovski (1964).

The area of the debonded zone is:

$$A = 2\pi a^2 (1 - \cos \theta_{\text{cavity}}) \tag{4}$$

When the debonded area increases by ΔA, the loss of elastic strain energy ΔW is:

$$\Delta W = U \left(\frac{\partial(\Delta V)}{\partial \theta_{\text{cavity}}} \right) \frac{\partial \theta_{\text{cavity}}}{\partial A} \Delta A = \frac{3k}{4\pi} Ua \sin(2\theta_{\text{cavity}}) \Delta A \tag{5}$$

Denoting G_a the adhesion energy by unit of surface, the detachment occurs when $\Delta W \geqslant G_a \Delta A$. In the frame of linear elasticity, the elastic energy density can be written as $U = \sigma^2/2E$, then from Eq. (5) we obtain the debonded angle θ_{cavity} as a function of the local stress σ_c:

$$\sigma_c = \sqrt{\frac{8\pi E G_a}{6a\sin(2\theta_{cavity})}} \tag{6}$$

The derivation of Eq. (6) assumes that the debonded elastomer between the cavity and the sphere is not strained, while the energy of the still bonded polymer ($\theta > \theta_{cavity}$) is not affected by the cavity. The initiation of the cavity is starting from a precursor θ_i, which is assumed to be small ($<5°$) and not disturbing the stress/strain relationship before debonding. It is taken to be an adjustable parameter, set to initiate the debonding at the same stress/strain as the experimental one. The physical meaning of this parameter corresponds to the way the first detachment is created: Cho and Gent have showed in 1988 that, under a sufficient triaxial stress, many closely spaced small cavities are created inside the elastomer, near the polar zone of the spheres. Indeed, elastomers are full of tiny gas inclusions or other small defects at the polymer/particle interphase, creating some vulnerable points. They may grow at the immediate vicinity of the poles of the particles till touching the surface of the particles, which leads to a debonding process.

2.1.3. Mechanical behaviour in the presence of a cavity

It is no longer possible to use the effective medium approach, as the characteristics of this zone will evolve with the strain. Moreover, neglecting its contribution does not bring a good agreement with the two spheres experiments. So, the stress contribution of this unrestrained elastomer has been calculated by assuming a rectilinear displacement field, associated with a determination of the cavity shape to compute the local strain. Moreover, according to experiments made on spheres embedded in a transparent elastomer, the debonding process will be described as the growth of only one cavity, at the surface of one sphere, till the polymer becomes detached from the equator of the particles, breaking this macroscopic system without initiating any other debonding.

To validate and set the required data, finite element calculations have been run. By giving access to the local stress, the debonded angle, the cavity shape, this helpful technique will be used to define an analytical shape of the cavity. In the simulation the debonded area is fixed at the beginning of the simulation and only the shape of this unrestrained area will change with the strain. For sake of simplicity, we have chosen to fit the shape of the cavity with an unique power law whatever the size of the cavity. The function defined by Eq. (7) is found to fit reasonably well the shape of the cavities obtained by numerical simulation (cf. Fig. 2a and b) till $\theta_{cavity} = 40°$:

$$f(r, \theta_{cavity}) = \left(\frac{u + a(1 - \cos\theta_{cavity})}{(a\sin\theta_{cavity})^{2,2}}\right) r^{2,2} + \frac{g}{2} \tag{7}$$

where u is the imposed displacement and g is the gap between the spheres of radius a.

Thus, the local stretch $\lambda(r)$ below the debonded area is given by (cf. Fig. 1):

$$\lambda(r) = \frac{f(r, \theta_c) + h(r)}{2h(r)} \quad \text{with } h(r) = \frac{g}{2} + a\left(1 - \sqrt{1 - \frac{r^2}{a^2}}\right) \tag{8}$$

Note that for $r = 0$, $\lambda(0) = 1$ meaning that at the apex of the cavity the elastomer is not strained. The stress of this unbounded elastomer below the cavity is calculated from Eq. (8), taking a Neo-Hookean behaviour of the pure elastomer:

$$\sigma_{cavity} = \int_0^{a\sin(\theta_{cavity})} \frac{E_m}{3}\left(\lambda(r) - \frac{1}{\lambda(r)^2}\right) \frac{2r}{(a\sin(\theta_{cavity}))^2} \mathrm{d}r \tag{9}$$

Always by comparing with the stress field given by FEM, the analytical stress is split in two independent contributions. Below the cavity, the stress is governed by Eq. (9), whereas the stress inside the bonded elasto-

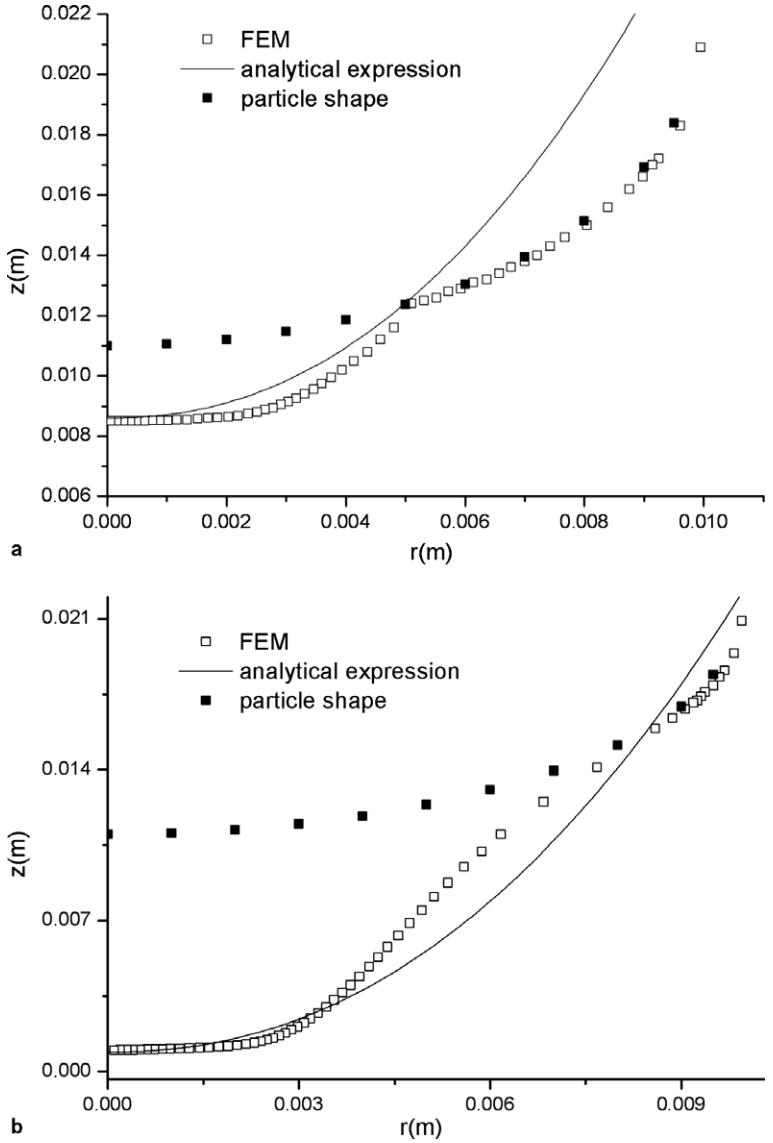

Fig. 2. (a) Polynomial fit of the cavity shape. $\theta_{\text{cavity}} = 30°$, $g/a = 0.1$, $\varepsilon = 3$. (b) Polynomial fit of the cavity shape. $\theta_{\text{cavity}} = 60°$, $g/a = 0.1$, $\varepsilon = 10$.

mer surrounding the cavity is calculated using the effective modulus of Eq. (1). Consequently, the stress/strain relationship for two close spheres, with one debonded area θ_{cavity}, is:

$$\sigma = \sin^2\theta_{\text{cavity}} \int_0^{a\sin(\theta_{\text{cavity}})} \frac{E}{3}\left(\lambda(r) - \frac{1}{\lambda(r)^2}\right)\frac{2r}{\left(a\sin\left(\theta_{\text{cavity}}\right)\right)^2}\mathrm{d}r + \left(1-\sin^2\theta_{\text{cavity}}\right)\frac{1}{4}E_{\text{m}}\varepsilon\frac{(2a+g)}{a} \times \int_{\theta_{\text{cavity}}}^{\frac{\pi}{2}} \frac{\sin^3\theta\cos\theta}{(g/2a+1-\cos\theta)^3}\mathrm{d}\theta \tag{10}$$

Fig. 3 shows a validation test of Eq. (10) by FEM calculation of a two spheres system. In the simulation the nodes initially on the surface between $\theta = 0$ and $\theta = \theta_{\text{cavity}}$ are free to move when the strain increases, whereas the nodes between $\theta_{\text{cavity}} \leqslant \theta_{\text{nodes}} \leqslant \pi/2$ have an imposed displacement equal to the sphere's one, building a

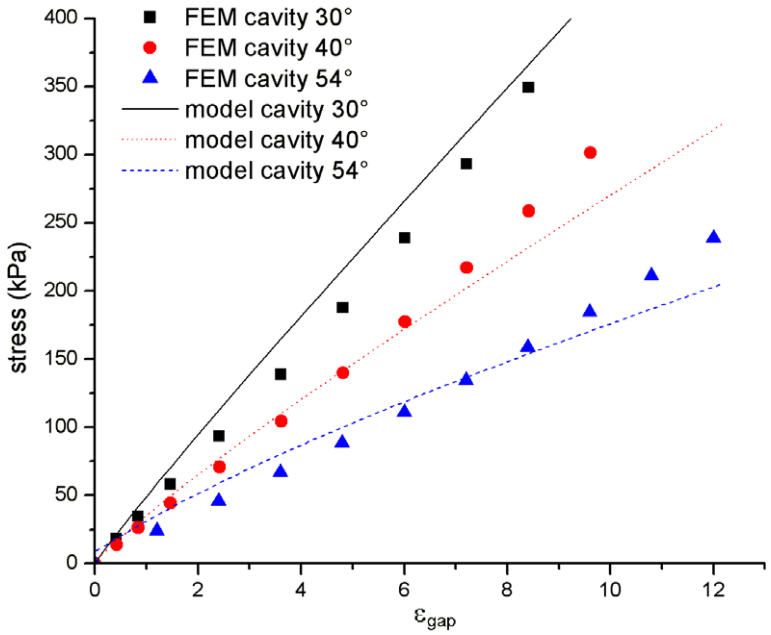

Fig. 3. Comparison of the analytical model with FEM, for an initially opened cavity; $g/a = 0.1$.

simulation where θ_{cavity} is constant whatever the strain. For each of the three angles ($\theta_{\text{cavity}} = 30°$, 40° and 54°), the model quite well agrees with the simulations.

In order to obtain analytically the stress/strain relationship of the debonding spheres, we calculate iteratively, by increasing step by step the strain. Once the critical stress is exceeded, the size of the cavity θ_{cavity} is recomputed at each strain by solving in θ_{cavity} the implicit equation. (11) based on the Griffith criteria (cf. Eq. (6)). The right-hand side of Eq. (11) is a function of the imposed displacement, u, and of the angle θ_{cavity} through $\lambda(r)$ given by Eq. (8). Then, the corresponding total stress is calculated using Eq. (10).

$$\sqrt{\frac{8\pi E_{\text{m}} G_{\text{a}}}{6a\sin(2\theta_{\text{cavity}})}} = \int_0^{a\sin\theta_{\text{cavity}}} \frac{E_{\text{m}}}{3}\left(\lambda(r) - \frac{1}{\lambda(r)^2}\right)\frac{2r}{(a\sin\theta_{\text{cavity}})^2}\,\mathrm{d}r \tag{11}$$

Finally, Eqs. (10) and (11) form a debonding model which takes into account only one parameter: the critical stress at which the abrupt debonding will appear (through the input of the size of initial defect $\theta_{\text{cavity}} = \theta_{\text{i}}$ satisfying Eq. (6) for the experimental value of σ_{c}). All the other data are either measured (for instance G_{a}), or set by the experimental device (spheres radius, gap). In particular, these equations will predict the stress jump during the first stage of debonding since its solution for the critical strain, $u = u_{\text{c}}$ gives the first value of θ_{cavity} and thus the associated stress given by Eq. (10).

2.2. Comparison with experiments on the two spheres system

In order to apply the model described in the preceding section, the adhesion energy G_{a} has to be measured; it has been realized with the help of an independent experimental device, where one iron plate is inserted between two other ones. Then, the elastomer is molded between the central plate and the two side plates which form a U and are connected to a force sensor. The iron plates are coated or not, following the same procedure as for the coating of the two spheres. This pull out test gives, respectively, $G_{\text{a}} = 700$ and 17 J/m^2 for coated and uncoated plates This value was derived by calculating the total elastic energy at rupture: $G_{\text{a}} = h\int_0^{\gamma_{\text{c}}} \sigma(\gamma)\,\mathrm{d}\gamma$ resulting from the quasi-equilibrium pull out test where h is the gap between the central plate and the two side plates.

2.2.1. Uncoated spheres

Experimentally, the creation of a debonded area clearly appears in Fig. 4 through a sudden decrease of the stress at $\varepsilon_{gap} = 40\%$. The evolution of the debonded angle has been obtained by FEM: we simulate the stress/strain curve with a cavity defined by a given angle θ_{cavity} and when the stress/strain curve crosses the experimental one we record the corresponding strain and indicate the angle θ_{cavity} at this strain on the upper side of the experimental curve. It indicates that the first macroscopic cavity obtained is 11° wide. This size corresponds to the position of the most stressed area, near the poles of the particles (Fig. 5). We have also found that for strains below $\varepsilon_{gap} = 40\%$ the maximum of the first principal strain is located at the surface of the particles, at 11° from the poles. Thus, we may expect the appearance of small cavities (microcavitation) and a debonding starting at this position and propagating immediately towards the pole where a second highly stressed area is located. The cavity angle can also be obtained directly from the analytical model (Eqs. (10) and (11)). The values are shown in Fig. 4 below the experimental curve. It appears that the analytical model predicts an initial cavity which is too large (20° instead of 11°) and a growth of the cavity with the strain which is too quick. It means that the evaluation of elastic energy in the Griffith criteria is a too crude approximation. All along the cavity increase, the stress map is strongly rearranged: whereas all the maxima stresses were near of the pole of the spheres before cavitation (cf. Fig. 5), the maximum principal strain is now located at the debonding tip (cf. Fig. 6 corresponding to $\theta_{cavity} = 30°$) and shows a large inhomogeneity of stresses: zero

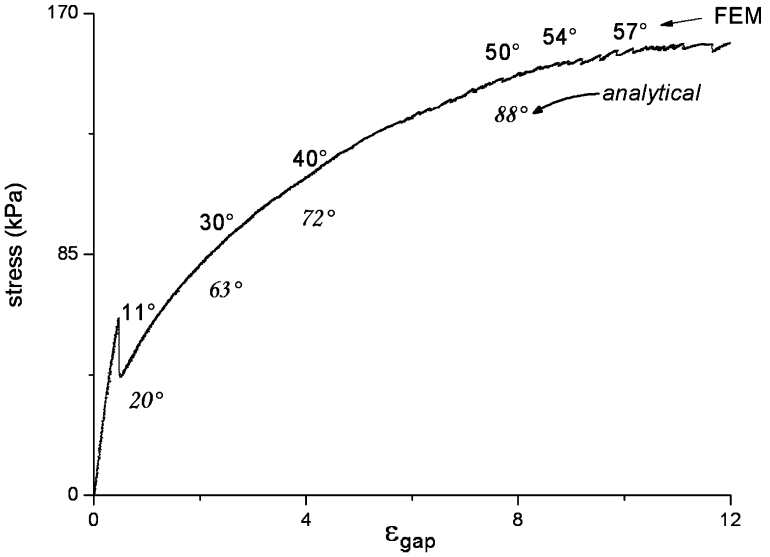

Fig. 4. Experimental curve for two uncoated spheres. $g/a = 0.1$; the cavity angles obtained for different strains are indicated along the stress/strain curve.

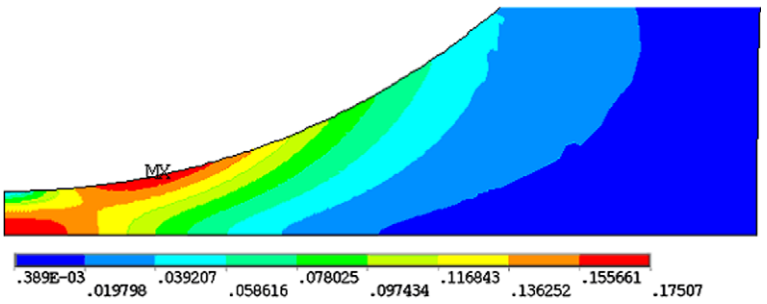

Fig. 5. Magnification of the FEM strain map in the pole region between two spheres (just before debonding). $\varepsilon_{gap} = 20\%$, $g/a = 0.1$; $\sigma_c = 140$ kPa.

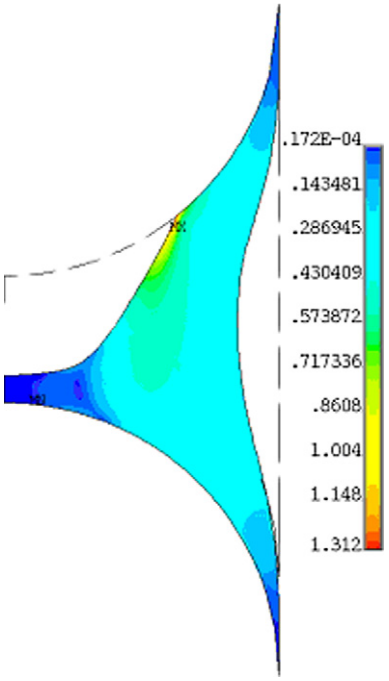

Fig. 6. FEM strain map for the two spheres system after debonding. $\theta_{\text{cavity}} = 30°$; $g/a = 0.1$.

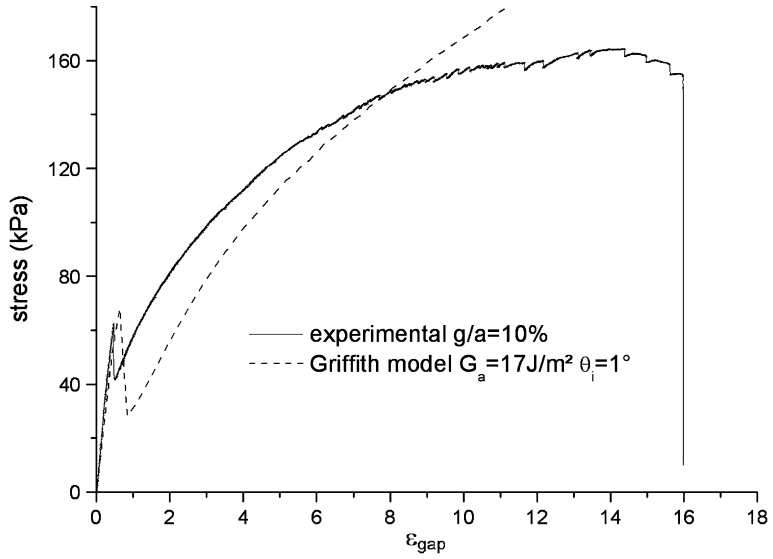

Fig. 7. Comparison between analytical theory and experiment for two uncoated spheres with $g/a = 0.1$.

at $\{r = 0, z = g/2\}$, 120 kPa at $\{r = a\sin\theta_{\text{cavity}}, z = 0\}$, 614 kPa on the border line of the cavity $\{r = a\sin\theta_{\text{cavity}}, z = (u+g)/2 + a(1-\cos\theta_{\text{cavity}})\}$ where it would tend to debond the elastomer. Note that the caving of the border line would not be present in the cell representing the composite since in that last case we impose it to remain straight. The equator remains almost not stressed till the cavity reaches $\theta = 90°$, where the cell is fully debonded and breaks. Despite the large disagreement on the cavity angle, we can see in Fig. 7 that the analytical model gives an acceptable agreement on the stress/strain curve till $\varepsilon_{\text{gap}} = 8$; beyond, the predicted cavity angle is close

to 90° and the result is meaningless in terms of degress. Note that the only parameter is the initial angle θ_i which is set to reproduce the critical stress of debonding; this angle is taken equal to 1° both for coated and uncoated particles.

2.2.2. Coated spheres

When elastomeric materials are highly stretched, a cohesive, internal failure takes place in the elastomer, at the midway of the poles of the particles (due to high triaxial stresses). Usually those cavities grow in the transverse direction of the loading till emerging from the gap, leading to a catastrophic growth and a breaking of the cell. Former studies made by Gent have shown that the macroscopic critical stress needed to create the cavitations was much lower in the case of two cavities than for a single inclusion: when the particles are closely spaced, one quickly gets high triaxial stresses. Those cavities are created from the unbounded expansion of microscopic voids, and their extension is governed by the tearing energy of the elastomer. In a general way, the modelling of this transverse growth of the cavity requires a different approach, as told by Yeoh (2002). However, the pull-out tests on grafted plates and the coated spheres experiments have lead to a breaking near the surface of the metal, in the polymer interphase rather than in the middle (we have detected by infrared reflection a thin elastomer layer at the surface of the plates). The same results were obtained for various adhesion primers (silane-based or commercial ones). This means that the failure process of the RTV1062 elastomer can just be described like a debonding that occurs at much higher stresses than the uncoated one. So, Eq. (12) can be used again to predict the growth of the cavity. The stress curve is presented in Fig. 8 together with the cavity angles obtained from a comparison with FEM simulation as described previously. It is seen that the initial cavity angle is now 30° instead of 11° for the weak bond case. This is due to the highest elastic energy stored in the elastomer before rupture. The prediction of the analytical model without any parameter ($G_a = 700\ \mathrm{J/m^2}$ is the adhesion energy measured with iron plates and $\theta_i = 1°$) is presented in Fig. 9. Here, the model overestimates by about 25% the decrease of stress during debonding, but well reproduce the softening of the traction curve after debonding.

2.2.3. Mullins effect on two spheres

It is worth looking how a previously partially debonded two spheres system behaves when it is stretched once more. Fig. 10 shows the first tension curve till a local strain $\varepsilon_{gap} = 6$ (well above the debonding) and

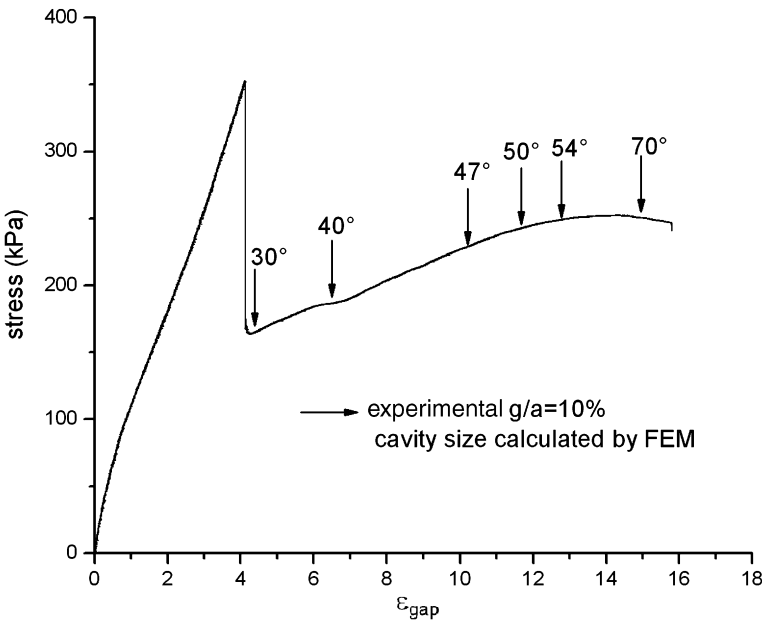

Fig. 8. Traction experiment for two coated spheres with $g/a = 0.1$; the cavity angles are those obtained from FEM simulations.

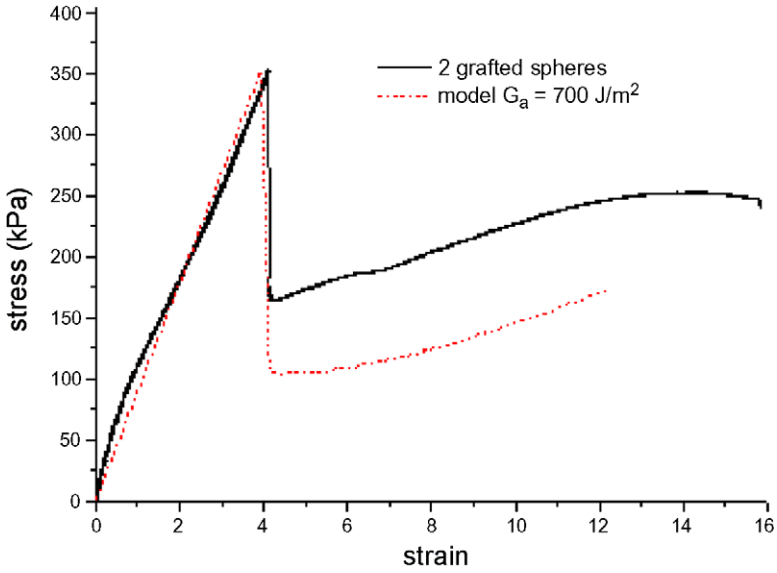

Fig. 9. Comparison between analytical theory and experiment for two coated spheres with $g/a = 0.1$.

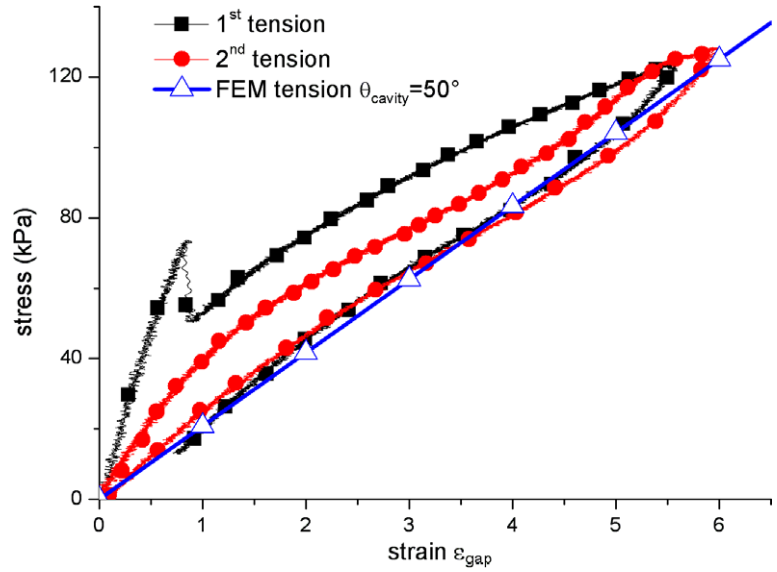

Fig. 10. Debonding and rebonding of a two spheres system.The empty triangles correspond to a simulation made with a cavity: $\theta_{cavity} = 50°$.

the retraction curve (return towards $\varepsilon = 0$). For this sample the stress at $\varepsilon_{gap} = 6$ corresponds to a FEM simulation done with a cavity having an angle $\theta_{cavity} = 50°$. We can note that this simulation (empty triangles) done with an angle of 50° well follows the experimental retraction curve, what is expected since it corresponds to the presence of a cavity whatever the strain is. However, the 2nd experimental tension curve (solid dots) is a bit different, as it stands between the 1st tension debonding curve and the retraction one. This means that when the elastomer is unstrained, some new adhesion with the iron surface takes place. This process of readhesion can play an important role for the energy dissipation under dynamic solicitations.

3. Stress/strain curves of the structured composite

A debonding model has been developed on a two spheres system; it must be transposed to the elementary cell of the structured composite. In this aim, the previously described two sphere system is now surrounded by an elastomer annulus of thickness L. Due to the neighbouring chains, the border of the cell, initially located at $r = a + L$, can move to ensure the compressibility of the unit cell, but has to remain straight (parallel to the chain axis). By replication of the unit cell along the structuring axis, a typical chain, representing the state of the composite, can be built, as following the paper of Moshev and Kozhevnikova (1995). This also highlights the importance of the gap, g, between two particles of a chain—or rather the ratio of the gap over the radius of the particles g/a—as a major parameter of the system. The model is described in more details in Coquelle et al., in press; we recall here that the thickness of the extra annulus, L, is set by the volume fraction ϕ of fillers:

$$a + L = \sqrt{\frac{4a^2}{3\varphi(2 + \frac{g}{a})}} \tag{12}$$

The displacement is constant everywhere on the two terminal-sections of the cylinder. It is set to zero on the bottom section, while it is equal to $\varepsilon(2a + g)$ on the upper one, $\varepsilon = u/(2a + g)$ being the imposed strain. Numerically, the lateral section is kept straight due to the presence of adjacent chains, but the average radius of the cylinder is allowed to decrease according to the Poisson ratio of the elastomer: $\Delta V = -\varepsilon V$. Finite element calculations have shown that the most strained regions were located near the poles of the particles (before debonding), and near the tip of the cavity (after failure). On the whole, the elastomer annulus which set by its thickness the volume fraction of charges can be seen as weakly stressed in comparison with the two spheres contribution. So, it can be assumed that both the cavity evolution and the corresponding stress would not change from the two spheres model to the elementary cell. FEM calculations of these two systems (2 spheres and elementary cell) gave a 10% difference on the stress and a 15% one on the debonded angle. Consequently, the stress on the elementary cell will simply be written as:

$$\sigma_{\text{cell}} = \frac{\sigma_{2\,\text{spheres}} a^2 + E_{\text{m}} \varepsilon_{\text{cell}} \left[(a + L)^2 - a^2 \right]}{(a + L)^2} \tag{13}$$

where $\sigma_{2\,\text{spheres}}$ is given by Eq. (10); L by Eq. (12) and $\varepsilon_{\text{cell}} = \varepsilon$.

The input data of the analytical model are the adhesion energy (measured), and the size of a small initial defect that will initiate the debonding process (referenced as θ_{i}). We will now show that, only using debonding process, the Mullins' effect can be predicted, at least for low strains, for those structured composites. We must assume here a similar behaviour for the macro- and the microspheres, as we have no measurement of the adhesion energy of the iron particles; we have chosen to take for the particles the same value of G_{a} as the one measured on iron plates (respectively, $G_{\text{a}} = 700\ \text{J/m}^2$ and $17\ \text{J/m}^2$ for coated and uncoated iron) and we have also taken for the debonding stress the one corresponding to the new radius of particles but with the same θ_{i} as for macroscopic spheres (cf. Eq. (6)). As already pointed out in the preceding paper, the grafting of silanes on the surface of the particles increases the difference of modulus that exists between the 1st tension of the grafted composite ($E = 750\ \text{kPa}$) and the uncoated one (420 kPa) for the same volume fraction of iron particles ($\sigma = 10\%$). We also assume that the elastomer does not have its mechanical properties changed in the gap region (as the particles may be very close) and that the chains of particles created by the field during the structuring process are as long as the sample. Consequently, as the debonding energy G_{a} (measured) and critical debonding stress (through θ_{i}) are taken equal to their macroscopic value, the only new parameter for the composite will be the gap between two particles, inside a chain.

Actually, in a perfect chain, all the links would debond at the same strain, that is surely not the case experimentally since we do not see any sudden change on the experimental stress/strain curve. So, in order to ensure a progressive debonding of the particles till high strains, we assume a Gaussian distribution of gaps; the mean gap g_0 and the standard deviation σ are then the two parameters obtained from the two first traction curves corresponding to grafted and non-grafted composites. The distances between particles inside a chain are calculated in the following way: first the gaps are set with a random Gaussian distribution, then for the 1st

tension, as long as the debonding critical stress, is not reached in one of the cell, the composite remains undamaged, and in each cell the modulus is given by Eq. (1). Then, as the material is more and more stretched, the local elastic stresses increases and reach, in one cell, the required value to initiate debonding. As a result, the stress of this cell is now given by Eq. (13), with $\sigma_{2\,\mathrm{spheres}}$ given by Eq. (10); for any further deformation, the cavity will grow, according to Eq. (11). As only low strains are considered, once the cavity reaches the equator of the particles, no further damage of the matrix is considered. For each increment, $\Delta\varepsilon$, of the total strain, the equilibrium position of each particle is searched with the condition that all the cells have the same stress and, of course, that the sum of each cell displacement is equal to the total displacement imposed on the chain:

$$\sigma_{\mathrm{cell},0}(\varepsilon_{\mathrm{cell},0}) = \sigma_{\mathrm{cell},1}(\varepsilon_{\mathrm{cell},1}) = \cdots = \sigma_{\mathrm{cell},N}(\varepsilon_{\mathrm{cell},N}) \tag{14}$$

$$\underbrace{\varepsilon_0 H_{\mathrm{cell},0}}_{u_0} + \underbrace{\varepsilon_1 H_{\mathrm{cell},1}}_{u_1} + \cdots + \underbrace{\varepsilon_N H_{\mathrm{cell},N}}_{u_N} = \underbrace{\varepsilon_{\mathrm{macro}} H_{\mathrm{cell,macro}}}_{u_{\mathrm{macro}}} \tag{15}$$

In Eq. (14) the stress dependence on the local strain is the one just described above. This iterative process is carried on: as the macroscopic stretch is increased, a new equilibrium configuration is searched (by equalizing the stresses of each cells), then the cells are checked for a second debonding, and so on. The debonding parameters are still an initial defect $\theta_i = 1°$, an adhesion energy of 700 J/m^2 for the grafted particles and 17 J/m^2 for the uncoated ones. A quite good fit of the experimental first tractions is obtained for $g_0/a = 3.8\%$, and a standard deviation $\sigma = 2.6\, g_0$ (Fig. 11). It must be pointed out that this model predicts a reasonable value for the average gap compared to previous determination supposing a perfect chain structure based on permeability measurement (De Vicente et al., 2002) or stress/strain curve which predicts $g_0/a = 5.6\%$ (Coquelle et al., in press).

Now, the behaviour of the material under a new tension (the 2nd tensions) will be different since some polymer-to-particle bonds have been broken during the first tension. We assume that even, if some bonds can partially reform, they open freely during the second tension. Therefore, this second traction curve is given by the stretch of N cells, among which a certain number, D, are already unbounded. This number D is obtained from the model at the end of the 1st tension. This difference between 1st and 2nd tension (i.e., the stress softening, known as Mullins effect) is mostly noticeable on the structured composites with grafted particles (Fig. 11, solid line) but, is almost negligible for the uncoated composite (difference between the solid and empty triangles) as

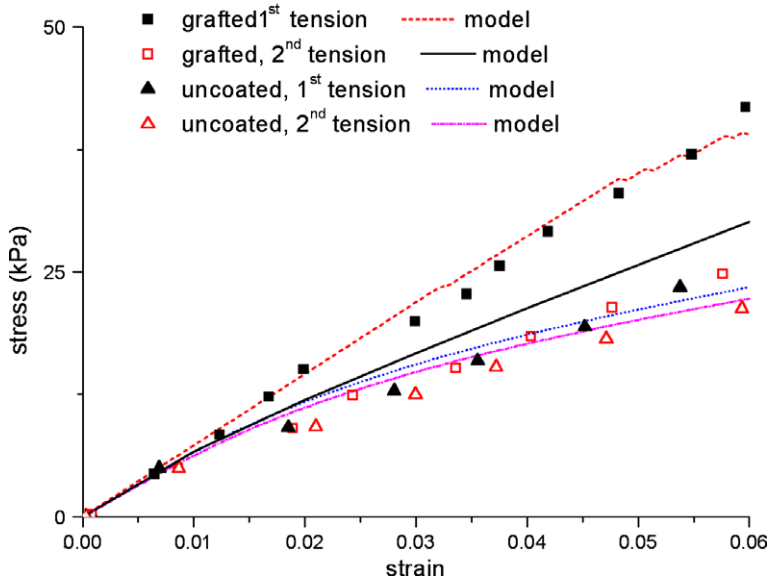

Fig. 11. Model and experimental curves of the structured composite, whose particles are coated (squares) or not (triangles). The volume fraction of iron is 10% in both cases.

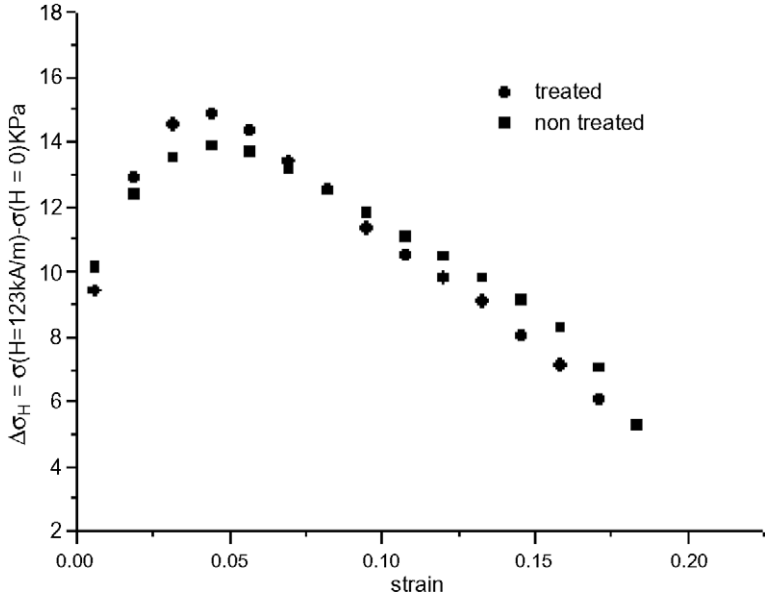

Fig. 12. Comparison of the magnetorheological effect between a composite whose particles are grafted to the matrix or not.

we could expect. Note also that the second tension of the coated sample is very close to the traction curve of the uncoated one; it means that during the first tension most of the particles have debonded.

In other words, coating the particles enhance the adhesion, but the particles are so close from each other that the debonding stress is reached since the lowest strains, opening so many cavities that the 2nd tensile modulus seems to dimly depend on the surface treatment of the particles. Concerning the uncoated composite, the difference between 1st and 2nd tension is tiny, meaning that it is quite as easy to open the cavity for the first time that to reopen it.

It is also important to note that the debonding between particles and elastomer should not influence the magnetorheological effect. Indeed, as the particles are organized in unidirectional chains, the application of a magnetic field induces an attractive force between particles that maintain them together till the elastic stress overcomes the magnetic one. The only effect of the coating could be indirect through its influence on the structure of the chains or the distance between particles. Actually, as shown in Fig. 12, there is almost no difference for the increase of stress in the presence of a field ($H = 123$ kA/m) between coated and uncoated particles.

4. Conclusion

The comparison between debonding experiments made on two spheres, FEM simulations and analytical model have shown that this latter was able to reproduce reasonably well the behaviour of the stress over the whole range of strain, including debonding.

The input data are the gap (set by the experiment), and the debonding stress (which is given by the adhesion energy measured by pull-out tests and the size of an initial defect θ_i (the only adjustable parameter of the model), which initiates the debonding process. This model has been able firstly to predict the stress drop, as a consequence of the initial growth of the cavity, and secondly the progressive diminution of the slope associated with the extension of the debonded cavity. Nevertheless the use of Griffith criteria tends to overestimate the size of the cavity.

In structured composites such as MRE, we have seen that the debonding process was playing a major role in the stress/strain relationship, particularly for coated particles. In this case, the debonding process results in a noticeable decrease of the Young modulus of the composite after the first traction that becomes similar to the one of the uncoated composite (around 420 kPa at $\phi = 10\%$).

The analytical model has been applied to the elementary cell of the structured composite, and extended to simulate the stress/strain relation on a chain of particles. In this last case the geometry of the chain was characterized by two parameters: the average gap and the width of a Gaussian distribution of gaps, which were adjusted to fit the first traction curve of the composites either coated or not. Then, when applied to the second traction, this model well predict the large Mullins effect in the case of strong bonds between particles and elastomer and the weak difference in the case of uncoated particles. At least it is shown that the increase of modulus due to the application of a magnetic field is not sensitive to the strength of these bonds between particles and matrix. Let us finally point that this model could be extended for planar strain, which is encountered in several practical applications. Nevertheless, in the most interesting case where the axis of the chains is situated in the plane of strain, we loose the cylindrical symmetry and a 3D model is needed; this problem will be addressed in a future work.

References

Bellan, C., Bossis, G., 2002. Field dependence of viscoelastic properties of MR elastomer. International Journal of Modern Physics B 16, 2447–2454.

Bossis, G., Coquelle, E., Kuzhir, P., 2004. Adaptive magnetorheological materials. Annales de chimie-Science des Matériaux 29, 6.

Carlson, J., Jolly, M., 2000. MR fluid, foam and elastomer devices. Mechatronics 10, 555–569.

Cho, K., Gent, N., 1988. Cavitation in model elastomeric composites. Journal of Materials Sciences 23, 141–144.

Christensen, R., 1979. Mechanics of Composite Materials. Wiley, New York, ISBN 0-89464-501-3.

Coquelle, E., Bossis, G., Szabo, D., Giulieri, F., in press. Micromechanical model of an elastomer filled with particles organized in chain-like structures. Journal of Materials Sciences.

De Vicente, J., Bossis, G., Lacis, S., Guyot, M., 2002. Permeability measurements in cobalt ferrite and carbonyl iron powders and suspensions. Journal of Magnetism and Magnetic Materials 251, 100–108.

Gent, A., 1980. Detachment of an elastic matrix from a rigid spherical inclusion. Journal of Materials Sciences 15, 2884–2888.

Gent, A., Park, B., 1984. Failure process in elastomers at near or a rigid spherical inclusion. Journal of Materials Sciences 19, 1947–1956.

Ginder, J., Nichols, M., Elie, L., Tardiff, J., 1999. Magnetorheological elastomers: properties and applications. SPIE Conference on Smart Materials Technologies, 131–138.

Huang, N., Korobeinik, M., 2001. Interfacial debonding of a spherical inclusion embedded in an infinite medium under remote stress. International Journal of Fracture 107, 11–30.

Kendall, K., 1994. Cracks at adhesive interfaces. Journal of Adhesion Sciences and Technologies 8 (11), 1271–1284.

Kraus, R., Wilke, W., Zhuk, A., Luzinov, I., Minko, S., Voronov, A., 1997a. Investigation of debonding process in particle-filled polymer materials by acoustic emission—Part I. Journal of Materials Sciences 32, 4397–4403.

Kraus, R., Wilke, W., Zhuk, A., Luzinov, I., Minko, S., Voronov, A., 1997b. Investigation of debonding process in particle-filled polymer materials by acoustic emission—Part II. Journal of Materials Sciences 32, 4405–4410.

Moshev, V., Kozhevnikova, L., 1995. Unit cell evolution in structurally damageable particulate-filled elastomeric composites under simple extension. Journal of Adhesion 55, 3–4.

Moshev, V., Kozhevnikova, L., 1997. Highly predictive structural cell for particulate polymeric composites. Journal of Adhesion 62, 169–186.

Moshev, V., Kozhevnikova, L., 2000. Predictive potentialities of a cylindrical structural cell for particulate elastomeric composites. International Journal of Solids and Structures 37, 1079–1097.

Moshev, V., Kozhevnikova, L., 2002. Structural cell of particulate elastomeric composites under extension and compression. International Journal of Solids and Structures 39, 449–465.

Mossakovski, Rybka, 1964. Journal of Applied Mathematics Mechanics 28, 1277.

Occhiuzzi, A., Spizzuoco, M., Serino, G., 2003. Experimental analysis of magnetorheological dampers for structural control. Smart Materials and Structures 12, 703–711.

Sohoni, G.B., Mark, J.E., 1987. Anisotropic reinforcement in elastomers containing magnetic filler particles. Journal of Applied Polymer Science 34, 2853–2859.

Yeoh, O., 2002. Relation between crack surface displacements and strain energy release rate in thin rubber sheets. Mechanics of Materials 34, 459–474.

Zhuk, A., Knunyants, N., Oshmyan, V., Topolkarev, V., Berlin, A., 1993. Debonding microprocesses and interfacial strength in particle-filled polymer materials. Journal of Materials Sciences 28, 4595–4606.